Research Square

Preprints are preliminary reports that have not undergone peer review. They should not be considered conclusive, used to inform clinical practice, or referenced by the media as validated information.

Pooled Human BM-MSCs and Hyaluronic Acid Restore Disc Matrix Homeostasis and Histological Architecture in a Rat Disc Degeneration Model of Lower Back Pain

Gyanoday Tripathi
National Institute of Pharmaceutical Education and Research (NIPER)-Ahmedabad

Komal Bhombe
National Institute of Pharmaceutical Education and Research (NIPER)-Ahmedabad

Priyabrata Sarangi
National Institute of Pharmaceutical Education and Research (NIPER)-Ahmedabad

Suresh Kannan
Stempeutics (India)

Pawan Kumar Gupta
Stempeutics (India)

Uday Kumar
Stempeutics (India)

Hemant Kumar
hemantbhave@gmail.com

National Institute of Pharmaceutical Education and Research (NIPER)-Ahmedabad

---

Research Article

Keywords: Intervertebral Disc Degeneration, Cell therapy, pooled hBM-MSC, Hyaluronic acid, Chondrogenesis

Posted Date: October 5th, 2026

DOI: https://doi.org/10.21203/rs.3.rs-11129159/v1

License: This work is licensed under a Creative Commons Attribution 4.0 International License. Read Full License

Additional Declarations: Competing interest reported. This study was supported by a research grant from Stempeutics Research PVT. LTD, which develops and commercialize the stem cell therapy

evaluated in this research. The authors confirm that the study adhered to established scientific and ethical standards. Beyond the disclosed research funding, the authors declare no additional personal associations, competing financial/non-financial interests that could influence the design, interpretation, or reporting of the study findings.

Abstract

In this study, we aim to evaluate the efficacy of pooled human bone marrow-derived mesenchymal stromal cells (hBM-MSCs) along with hyaluronic acid (HA) termed as Stempeucel®. In a lateral incision disc puncture induced rat model of intervertebral disc disease. Using a lateral incision approach, a 22-gauge needle was employed to puncture the lumbar discs (L5-L6), inducing nucleus pulposus (NP) cell degeneration and promoting hallmarks of degenerative features, including degenerated chondrocyte like NP cells and increased tissue fibrosis. Disease progression was evaluated at weeks 4, 8, and 12. We further investigated the efficacy of pooled hBM-MSCs delivered in combination with HA hydrogel carrier. Three human equivalent doses (HEDs) of hBM-MSCs (5, 10, and 15 million cells) were injected intradiscally. The combination therapy significantly preserved disc structure and promoted tissue regeneration. Notably, by week 12, treated discs showed improvements in pain reduction, and histological parameters. Elevated expression of aggrecan, SOX9, and collagen-II, indicating enhanced chondrogenesis. The treatment promoted recovery of NP cells, resulting in enhanced proteoglycans that are crucial for disc hydration and function. The treatment mitigated fibrotic changes induced by the needle puncture, suggesting a reversal of degeneration. This study presents the regenerative potential of pooled hBM-MSCs and HA for treating IVDD, offering a promising strategy for long-term relief from LBP.

Introduction

Intervertebral discs (IVDs) are the soft, cushion-like structures between the spine's vertebrae. They consists of a tough outer layer called the Annulus Fibrosus (AF) and a gel-like inner core nucleus pulposus (NP) (Shapiro and Risbud 2016). Intervertebral disc Degeneration (IVDD) is a common condition which arises from various factors, including aging, trauma, genetic predisposition, and lifestyle factors such as smoking and obesity. These factors lead to the loss of water content, cellular hypertrophy, reduced chondrogenesis, and dedifferentiation of the NP cells (Zhang et al. 2020; Lin et al. 2019a), as well as thinning and tearing of the AF. These degenerative changes contribute to impaired disc function and are often associated with lower back pain (LBP) (Diwan and Melrose 2023). LBP is a prevalent and a leading cause of long-term disability that poses a significant financial burden on society (Alfalogy et al. 2023). The precise etiology of LBP is poorly understood, IVDD is recognized as a primary contributor. IVDD is characterized by notable morphological changes, which may result from aging (Yang et al. 2020), mechanical stress, or trauma (Alkhatib et al. 2014). Current therapeutic strategies for IVDD primarily focus on alleviating pain rather than addressing the underlying pathological processes. These approaches include conservative management, and pharmacological interventions; as well as more invasive treatments like epidural steroid injections, disc replacement, and spinal fusion (Binch et al. 2021). Nevertheless, these modalities are predominantly symptom-alleviating rather than disease-modifying, providing temporary relief but offering limited or no sustained long-term benefits in halting or reversing the pathology.

Mesenchymal Stromal cells (MSCs) comprise a heterogeneous population residing within diverse stromal tissues, capable of differentiating into chondrocytes, adipocytes, myocytes, and osteocytes,

representing multilineage mesenchymal differentiation potential contributing to tissue regeneration and repair. Recent advancements in regenerative medicine, particularly the use of MSCs, offer promising therapeutic potential for treating IVDD (Steffen et al. 2017). MSCs are known to adhere to plastic surfaces, have spindle-shaped morphology, and express specific surface markers positive for (CD 90, 73, 105 and negative for CD 34, 45), as defined by International Society for Cellular Therapy (ISCT) (Widjaja et al. 2022). MSCs possess the capacity to differentiate into multiple mesodermal and non-mesodermal lineages when exposed to suitable microenvironmental cues. MSCs exert their therapeutic effects primarily through paracrine signalling, releasing various growth factors and cytokines that modulate the local microenvironment (Kusuma et al. 2017). Bone marrow-derived MSCs (BM-MSCs) are particularly favoured in clinical applications due to their accessibility, ease of extraction, and suitability for both autologous and allogeneic treatments (El-Jawhari et al. 2021). However, the therapeutic efficacy of MSCs can vary significantly due to heterogeneity, including differences in sex, age, health status, and genetic makeup (Česnik and Švajger 2024; Ouzin and Kogler 2023). To address these challenges, pooling MSCs from multiple donors has been proposed as a strategy to enhance therapeutic consistency and efficacy. This approach combines cells with diverse therapeutic properties, potentially mitigating the limitations associated with single-donor MSCs and enhancing overall therapeutic potential (Kannan et al. 2024; Willer et al. 2022). hBM-MSCs were chosen for their regenerative, anti-inflammatory, and extracellular matrix (ECM) remodeling properties (Di Sarno 2022; O'Connor 2019).

The aim of this study lies in following objectives; (i) evaluating whether pooled MSCs improve consistency of regenerative response in IVDD (ii) assessing dose-dependent efficacy using clinically relevant human-equivalent dosing and (iii) investigating ECM remodeling and hypertrophy reversal mechanisms at the tissue level with 12-week functional and histological follow-up.

Materials and Methods

Preparation and characterization of Pooled hBM-MSCs

Bone marrow was obtained from healthy male donors aged 20–35 years following written informed consent. Aspiration was performed from the posterior iliac crest, and mononuclear cells (MNCs) were isolated. The procedure was approved by the Institutional Ethics Committee (IEC) of Kasturba Hospital, Manipal, Karnataka (Approval No. SRPL/CLI/07–08/001). The MNCs were expanded, and cells from three independent donors were pooled at passage 1, then further expanded to passage 3. For the final product, the Working Cell Bank (WCB) were further expanded up to passage 5 prior to use. Pooling was performed to minimize donor-to-donor heterogeneity and to generate MSCs with more consistent secretory activity and enhanced immunomodulatory potential, as supported by recent evidence (Kannan et al. 2024). The pooled cells were cryopreserved at concentrations of 5M/ml, 10M/ml, and 15M/ml. These cells were characterized for viability, viable cell count, phenotypic markers, and trilineage differentiation potential before using for the *in vivo* study **(Supplementary Table 1)**. Phenotypic characterization was performed according to ISCT minimal criteria MSCs. **(Supplementary Table 2)**. For analyzing trilineage differentiation, MSCs were cultured in ready-to-use adipocyte, osteocyte, and

chondrocyte differentiation media (Invitrogen-Gibco). The differentiation was confirmed after staining them with Oil Red O, Alizarin Red S, and Safranin, respectively **(Supplementary Fig. 1)**.

Needle size selection

We performed a pilot study to determine the optimal needle size for inducing the necessary disc injury and select the appropriate needle gauge for the efficient delivery of Stempeucel®. To select an appropriate needle size for the ease of delivery of Stempeucel® into the rat lumbar disc, we tested different gauge (G) sizes ranging from 18G, 20G, 22G, and 26 ½ G. The 18G and 20G needles, being relatively large in diameter, likely caused excessive damage to the disc tissue during insertion. This excessive tissue disruption can lead to greater degeneration of the disc and may compromise the model's accuracy in simulating disc conditions. Additionally, the larger needle size might increase the risk of leakage of the injected material, reducing the precision of the delivery. The 26 ½ G needle, being much smaller in diameter, would minimize tissue damage. However, its small size may present difficulties in delivering an adequate volume of Cells into the disc. The fine needle might also increase the risk of clogging or incomplete delivery, leading to inconsistent or suboptimal administration of the cells. Additionally, the small gauge could be less effective at creating the necessary degree of disc damage needed to develop the model. We observed that the 22G needle is the optimal gauge size for both creating the model and delivering MSCs, providing an appropriate range of disc damage.

Animals and Standard Conditions

Male and Female Sprague Dawley rats (12–15 weeks old, 350–450 g) were used. The animals were housed under controlled environment, with a 55–65% humidity and at 24 ± 2 ℃ temperature with a cycle of 12 h light and 12 h dark and free access to a pelleted commercial diet and water. All surgical procedures were conducted in accordance with ethical guidelines and were approved by the Institutional Animal Ethics Committee (NIPERA/IAEC/2023/018) at NIPER Ahmedabad, India.

Needle puncture (Lateral Incision)

After one week of acclimatization feeding, the rats were used for model construction, ensuring that all animals selected for surgery were in optimal health prior to the procedure. Animals were divided into six groups, as follows: Sham, Needle puncture (PlasmaLyte A, Baxter-FE0324), HA only (Hyalgan® 20 mg/2 mL, MW 500,000–730,000 Da), 5M, 10M, and 15M Stempeucel® (PlasmaLyte+ Cells/HA) (n = 6/group) **(Supplementary Table 3)**. Surgical procedures were followed as per the previously reported literatures (Oehme et al. 2012; Cheng et al. 2021). Briefly, animals were anesthetized by a combination of ketamine (75 mg/kg) and xylazine (10 mg/kg) half an hour prior to surgery. Hair was removed adjacent to lumbar region; the surgical site was cleaned with absolute alcohol and povidone-iodine. A longitudinal incision was made adjacent to the vertebral column (1.5 cm) at a depth of up to 10 mm. Excessive muscles were removed until the disc could be visualized. The disc at the L5/6 level was punctured with a 22G needle to

a depth of 2 mm, followed by a 360˚ rotation maintained for 30 seconds. For the treatment group(s), 10 µL of Stempeucel® was injected intradiscally **(**Fig. 1b**)**. Following cell injection, the muscle layer was closed with 4 – 0 sutures, and the skin was sutured using 2 – 0 sutures to ensure proper wound closure. Post-operative care with 0.3 mg/kg buprenorphine (OD), followed by 5 mg/kg gentamicin, was administered for up to 1 week.

Administration of cells (Dose used)

The conversion of treatment doses from human to rat and the concentrations required for rat injections were calculated. The human dosages given are 5M, 10M, and 15M; these values represent the dosage per kilogram for a human weighing 60 kg. Using a conversion ratio of 6.2, the human dosage was converted to an equal rat dosage. The dosage required for a 400-gram rat is calculated and resuspended in 5 µL. For injection, the resuspended cells (5 µL) are mixed with PlasmaLyte and HA **(Supplementary Table 4)**.

Behavioral Studies

Body weight assessment

To investigate the impact of needle puncture on body weight and to determine whether subsequent treatment with Stempeucel® could reverse any effects, we measured the body weight of all the animals from each group at day 0 for basal reading, followed by days 3, 7, 11, 14, 21, 28, 42, 56, 70, and 84 **(Supplementary Table 5)**.

Tail Flick (Tail base)

Thermal hyperalgesia was studied using tail flick analgesiometer (Columbus instruments), where a radiant heat stimulus (IR light) were exposed to the ventral part of the tail base (Lee et al. 2009). Before applying the radiant heat, animals were acclimatized for 30 seconds. 10 seconds were kept as cut-off time. The withdrawal latency was observed and differences calculated on weeks 1, 2, 4, 6, 8, 10, and 12. **(Supplementary Table 6)**.

von Frey (Injury site/Lumbar region)

To evaluate the mechanical allodynia, von Frey filaments were employed on weeks 1, 2, 4, 6, 8, 10, and 12 **(Supplementary Table 7)**. Rats were habituated for 15–20 minutes prior by placing individually in a compartmentalized enclosures with wire mesh floors. The test was conducted using a 2 g filament to apply force at a specified site. A positive response was defined as animal exhibiting behaviors such as flinching, licking, or withdrawal upon filament application. A negative response was recorded if the animal showed no reaction, after which a higher-weight filament was applied. Upon a positive response,

testing proceeded with a lower-weight filament. Then, we calculated the withdrawal threshold according to SUDO method (Bonin et al. 2014; Glaeser et al. 2020).

Pinch meter (Hind paws)

The paw pressure test was used to determine response thresholds to mechanical pressure stimulation for measuring mechanical hyperalgesia, involving the application of gradually increasing force to the paw until withdrawal, vocalization was elicited (Jiang et al. 2023). The Randall-Selitto test was performed by a hand-held device (Paw Pressure Test Apparatus, IITC). Animals were restrained in a towel that provided access to the hind paws, and then animals were habituated to the restraint method and the apparatus. Mechanical pressure is gradually applied to the plantar surface of the hind paw until a nociceptive response occurs. The withdrawal response was recorded in same apparatus, providing an objective quantification of the mechanical pain sensitivity. The cut-off threshold was kept at 250 g. Differences in the withdrawal threshold were observed and calculated at weeks 1, 2, 4, 6, 8, 10, and 12 **(Supplementary Tables 8 & 9)**.

Footprint analysis

Footprint analysis was used to assess the gait behavior and motor coordination (Olby et al. 2020). These parameters were evaluated on weeks 1, 4, 6, 8, 10, and 12, following the needle puncture and after Stempeucel® treatment using the manual method **(Supplementary Fig. 2)**. The fore and hind paws were marked with inks of distinct colours (blue and red, respectively), then the animals were placed on absorbent paper enclosed within a cage border. To promote linear locomotion, a stimulus was presented at the endpoint. The resulting footprint patterns were digitized, and representative images were analyzed to evaluate motor coordination.

Staining and Immunohistology

For staining and immunohistology, animals were anesthetized at week 12, followed by transcardial perfusion with 0.9% saline and 4% paraformaldehyde (PFA) to fix the tissues. The vertebral column from the lumbar region containing the injury epicenter was excised and post-fixed in PFA at 4°C for 24 hours. Samples were then decalcified in a decalcifying solution (Sigma, D0818-1L) for 18–20 hours. After tissue processing through ascending ethanol series, paraffin embedding was performed in paraffin embedder (Thermo Fisher, Histostar A81000002, USA). Further, longitudinal 5 µm thickness tissue sections were prepared through microtome (Leica, 14051856372, Germany).

Hematoxylin and Eosin (H&E) staining

To visualize the architecture of disc following IVDD, we performed H&E staining at 12 weeks using a commercially available kit (Abcam, ab245880, UK). After rehydration, tissue sections were stained for 1 minute with hematoxylin and rinsed with tap water, followed by dipped in blueing reagent for 10 seconds. Then for 6 minutes sections were counterstained with eosin and washed 3 times with absolute alcohol for 30 seconds each. Finally, the slides were mounted using DPX (Sigma, 06522). Furthermore, the histological grading of stained sections were performed based on the histological classification criteria

(Lai et al. 2021). Briefly, the scoring was recorded on the basis of cellularity and morphology of the disc, boundary between NP and AF, and the structural appearance of endplate morphology (scores 0–2). Based on the established grading criteria, score of 0 corresponds to a healthy disc, 1 to mild degeneration, and 2 to severe degeneration. The total histological score ranges from 0, indicating a normal disc, to a maximum of 16, representing severe degeneration. Histological specimens were subjectively evaluated for tissue morphology, structural integrity, and histological score by researchers who were blinded to the specimen identities.

Safranin O/ Fast Green Stain (SOFG)

SOFG were performed to examine proteoglycan-specific cartilaginous or glycosaminoglycans (GAG) content after IVD degeneration (Lü et al. 1997) at 12 weeks. Briefly, after defatting the slides, followed by rehydration with gradient ethanol and distilled water, sections were immersed in hematoxylin for 30 seconds and rinsed with running tap water. Then, the sections were dipped in 0.02% Fast Green Solution (F7258) for 6 minutes, followed by 1% acetic acid for 10 seconds. The sections were then directly immersed in 1% Safranin-O solution (S8884) for 5 minutes. Following that, sections were dehydrated in absolute alcohol for 1–2 minutes. Subsequently, the slides were mounted. Furthermore, the GAG content (stain intensity) was analyzed through image J, following an ROI were created through free hand tool, then the selected areas were subjected to histogram analysis, then selected the RGB box, and changed the notation of selected image from intensity (un weighted) to Red which is similar to (safranin) colour. Mean intensity values were subsequently recorded for further analysis.

Masson’s Trichrome Staining (MT)

We performed the MT staining to identify the muscle fibers, collagen, and connective tissues of the IVD (Leung et al. 2009; Gruber et al. 2005) after degeneration at 12 weeks using the Merck Masson-Goldner staining kit (1.00485.0001, Merck) as per manufacturer instructions. After defatting and rehydration, the sections were exposed for 1 minute with hematoxylin and washed with running water (3 minutes). Slides were rinsed for 30 seconds with 1% acetic acid, followed by 6 minutes in Azophloxin solution, then washed again with 1% acetic acid for 30 seconds. Subsequently, sections were dipped for 1 minute in Orange G solution and rinsed with 1% acetic acid. This was followed by staining with Light Green SF solution for 2 minutes, after which the slides were washed again with 1% acetic acid for 30 seconds. The sections were then dehydrated through a graded series of ethanol (70%, 96%, and 100%) each for 30 seconds and mounted the slides using DPX. Furthermore, the percentage area of collagen (fibrocartilaginous area) was quantified using ImageJ software. Image files were first opened and processed using the Colour Deconvolution plugin with the *Masson’s Trichrome* setting. From the resulting deconvoluted channels, the relevant collagen-specific (uncoloured) image was selected. Thresholding was then applied to correct background variability based on a reference image. Particle analysis was subsequently performed by selecting the parameters, including display results, summarize, and exclude on edges. The mean percentage area values were then calculated for further quantitative analysis.

Immunohistochemistry (IHC)

For IHC, deparaffinized the sections in xylene and a graded descending series of ethanol were used for rehydration. Subsequently, the sections were incubated with primary antibodies **(Supplementary Table 10)** at 4 ˚C for overnight. Next, following washing with Tween 20 (1% in PBS) sections were incubated with secondary antibodies **(Supplementary Table 11)** for 1 hour at room temperature. The sections were then incubated with DAPI (Sigma, D9542) diluted 1:1000 in 1× PBS for 10 minutes. Following incubation, the sections were mounted with DPX mountant, and imaging was performed using a confocal microscope. Then, the ROI subset was created in ZEISS (ZEN 3.9) software and quantified the fluorescence intensity in ImageJ software for all the experimental groups.

Biodistribution (BD) Studies

The BD studies using histopathology and IHC were performed to examine biodistribution and toxicity of Stempeucel® at both target and non-target sites.

To evaluate biodistribution and toxicity of MSCs, H&E staining was performed at weeks 1, 2, and 4. A total of 6 rats (2 animal/time point) were divided into 2 groups, including HA only, and 15M. A dose of 10 µL of HA was administered in HA only group and a dose of 15M cells were injected in Stempeucel® group. The 15M were prepared in 10 µL PlasmaLyte (vehicle) and injected intradiscal into the lower lumbar (L5-L6) IVD. Subsequently, the administered site was checked to ensure there is no leakage post injection. On days 7, 14 and 28 after injection, 2 animal/time point from each group were anesthetized by intraperitoneal injection of ketamine and xylazine, the animals were perfused transcardially with 100 mL of saline following 100 mL of 4% paraformaldehyde. Subsequently, various tissues including brain, heart, lung, liver, kidneys, spleen, ovary, spinal cord, and IVD were harvested for further processing.

Assessment of the presence of Stempeucel® at weeks 4 and 8 using labelled cells

To examine the presence of Stempeucel® in to the rat disc at weeks 4 and 8, immunohistochemistry of human nuclear antigen (HuNu) and DiO (468495-100MG) was performed on 8 rats. Groups at week 4 including needle puncture, 10M, and 10M + DiO, and for week 8, needle puncture, 15M, and 15M + DiO, followed by histological assessment through H&E, SOFG and MT staining.

Statistical analysis

All data are presented as mean ± standard error of the mean (SEM). Statistical analyses were conducted using GraphPad Prism software (version 8.0). Measurement data were analyzed using ordinary one way and two-way analysis of variance (ANOVA), followed by Tukey’s post hoc test for comparisons among three or more groups. The p values are given in the captions of respective figures.

Results

Characteristics of pooled MSCs

Cryopreserved pooled BM-MSCs, upon thawing, showed consistently high post-thaw viability across all three tested concentrations (5M/mL, 10M/mL, and 15M/mL), with viability percentages exceeding 80% in all samples. Similarly, the viable cell recovery was above 80% for each batch, indicating that the pooling and cryopreservation process preserved cell integrity effectively. Flow cytometry analysis of pooled MSCs confirmed the expected immunophenotype. More than 90% of the cells expressed the MSC-specific positive markers CD73, CD90, and CD105, while the expression of hematopoietic lineage-negative markers CD34 and CD45 was below 10%, in compliance with ISCT minimal criteria.

The trilineage differentiation assay demonstrated that pooled BM-MSCs retained their multipotent capacity post-expansion and cryopreservation. Adipogenic differentiation was evidenced by intracellular lipid droplet accumulation stained with Oil Red O; osteogenic differentiation was confirmed by extensive calcium deposition visualized by Alizarin Red S; and chondrogenic potential was shown by the presence of cartilaginous matrix components stained with Safranin O **(Supplementary Fig. 1)**. Collectively, these results validate the functional and phenotypic characteristics of the pooled hBM-MSCs for further pre-clinical applications.

No significant alterations in body weight following needle puncture and subsequent treatment with Stempeucel®

No significant differences were observed in baseline body weight among the animals. Furthermore, all groups showed typical variations in body weight, with no notable changes due to the injury. Similarly, animals in the treatment group showed consistent body weight trends following needle puncture and delivery of Stempeucel®, showing that the intradiscal administration of Cells did not cause any systemic adverse effects (Fig. 1c).

Higher doses of Stempeucel® significantly reduce pain perception, enhance gait behavior, and improve histological features in the later stages of injury

Animals from the needle puncture and Stempeucel®-treated groups exhibited a non-significant trend toward reducing thermal hyperalgesia. While an increase in latency with higher doses at a later time point was observed. In case of mechanical allodynia, the needle puncture group showed a significant withdrawal threshold at week 6 following reversal with treatment of Cells. Thereafter, no significant trend was observed until week 12. Mechanical hyperalgesia in the hind paw of the Stempeucel®-administered group following the needle puncture resulted in significant improvements from week 3 to week 12. The footprint data suggest that after needle puncture, all animals exhibited significant impairments in motor coordination during forepaw-hind paw stepping. However, those treated with 10M and 15M demonstrated marked improvements in gait and motor coordination compared to untreated group. Whereas the sham animals remained unchanged throughout the testing period (Fig. 2a-d).

To evaluate the effect of Stempeucel® on the histological features of the disc after needle puncture, we performed several staining techniques. The H&E staining results indicate that high doses of Stempeucel® lead to significant morphological improvements characterized by enhanced structural

integrity, as confirmed by histological scoring. Additionally, a marked elevation in proteoglycan contents suggests enhanced ECM composition. Furthermore, we observed reduced fibrocartilaginous content in NP region. These findings demonstrate the promising role of high-dose Stempeucel® in cartilage regeneration at the later stages of injury (Fig. 2e-f).

Effect of high-dose Stempeucel® on proteoglycans, chondrogenesis, and fibrosis

Immunohistology of Col-I, II, ACAN, TSK, and SOX9 was done to examine the therapeutic effects of Stempeucel® following needle puncture of the rat disc. Statistical data demonstrate that treatment with high doses of Stempeucel® significantly increases the expression of col-II and reduces tissue fibrosis, thereby mitigating the adverse effects associated with excessive cell enlargement (Fig. 3a-c).

Moreover, a notable elevation in proteoglycan levels indicates improved ECM composition. A marked chondrogenesis was also observed, pointing to increased cartilage formation or chondrogenesis. Finally, the treatment promoted substantial tissue regeneration, highlighting the potential of high-dose Stempeucel® therapy in NP repair and regeneration (Fig. 4a-f).

Absence of tissue abnormality in experimental group, implying nontoxic effects of Stempeucel®

There are no alterations in morphology of all the isolated tissues; Brain (intact cortical neurons), Heart (well oriented morphology of the cardiomyocytes), Lung (no alterations in lung cell structure like cell swelling, shrinkage, or the presence of inflammatory cells infiltrating the alveolar spaces), Liver (well-organized hepatocytes arranged in hepatic lobules with distinct nuclei and a uniform cytoplasm, no signs of damage or toxicity in hepatocytes), Kidneys (no swollen or necrotic tubular cells, disrupted glomerular structures, or inflammatory cell infiltration), Spleen (no parenchymal and capsular fibrosis), Ovary (no stromal alterations like fibrosis edema, no sign of pyknotic nuclei of ovarian tissue), Spinal cord (no morphological abnormality or neuronal damage). Along with these characteristics, IVD of experimental animals exhibited a healthy and normal histological feature **(Supplementary Fig. 3)**.

Furthermore, histological analysis revealed distinct variations in morphology, proteoglycan content, and collagen fiber organization among the sham, PlasmaLyte, 10M, and 10M + DiO groups at week 4, as well as in the 15M and 15M + DiO groups at week 8 (Fig. 5a-b). Additionally, immunohistochemical staining for HuNu and DiO demonstrated a higher expression in discs treated with 15M cells at week 8 compared to those treated with 10M cells at week 4. Moreover, a higher expression of HuNu at days 7, 14, and 28, in the IVDs compared to those treated with HA only groups (Fig. 5c-e).

Discussion

LBP is a prevalent health condition that places a significant financial burden on society and leads to long-lasting disability (Chen et al. 2022). It represents a major socioeconomic challenge in the United

States, contributing to approximately 100 million lost workdays each year, with associated costs estimated between $560–630 billion annually (Samanta et al. 2023). Despite the exact origin of LBP being frequently unknown, IVDD is a primary source of LBP, characterizing evident morphological changes that are caused by trauma, aging, or mechanical stress (Koroth et al. 2023). In advanced stages of disc degeneration, NP cells exhibit marked downregulation of matrix components, loss of small and large proteoglycans, which leads to reduced chondrogenesis, stiffening of NP cells, increased fibrosis, and ultimately disc degeneration (Lin et al. 2019b). Consequently, there is a critical need to develop more effective and regenerative therapeutic approaches for managing IVDD. Advances in regenerative medicine, particularly hBM-MSCs, have shown significant therapeutic potential (Gómez-Barrena et al. 2018).

This study aims to evaluate the improve consistency and regenerative response of pooled MSCs, further to assess dose-dependent efficacy using clinically relevant human-equivalent doses and to investigate matrix homeostasis and remodeling mechanisms at the tissue level with 12-week follow up. Next, to develop a reliable and safe approach for establishing an *in-vivo* model to allow precise induction of disc injury while providing a straightforward and accessible route for evaluating novel therapeutic strategies. Additionally, this model was employed to investigate the therapeutic outcomes of Stempeucel® in mitigating disc degeneration. The pilot study was conducted to address a significant challenge: selecting an appropriate needle size for cell delivery and establishing an optimal surgical approach. The 22G needle is better for both creating the model and for delivering the Cells with an appropriate range of damaging the disc. The lateral incision needle puncture method was selected due to its reduced risk of spinal cord damage and better outcomes. We evaluated the varying dosages of Stempeucel®, i.e., HED 5M, 10M, and 15M cells in the main study.

Stempeucel® alleviates pain perception and significantly improves histological features, with more pronounced therapeutic effects observed in the higher dosage group. In the needle puncture-induced IVDD, animals exhibit altered behavioral and histological parameters indicative of discogenic pain and functional impairment (Lai et al. 2015; Bergmann et al. 2022). These changes include increased sensitivity to mechanical and thermal stimuli, decreased locomotor activity, and altered gait patterns (Gorney et al. 2016). Such behavioral alterations reflect the onset and progression of pain associated with disc degeneration, mimicking clinical symptoms. The performed behavioral tests in this study indicated significant pain alleviation in the pinch meter and improved motor function in the treated groups compared to the needle puncture groups. Histopathological analysis showed preservation of NP integrity, proteoglycans, and reduced fibrocartilaginous content into the NP region in the treatment groups, particularly with higher doses of formulation. Stempeucel® upregulates the expression of NP matrix components Col-II and chondrogenic marker SOX9 in NP cells during the later stages of injury. In the needle puncture group, there is a marked reduction in the expression of key NP matrix components, particularly Col-II at week 12, which is essential for maintaining disc structure and function (Chou et al. 2003). This decline is accompanied by impaired chondrogenesis in NP cells (Khalid et al. 2023), reflecting a shift away from their native phenotype and contributing to the progressive deterioration of the ECM (Penolazzi et al. 2022). The reduced Col-II expression not only compromises the biomechanical

properties of the disc but also indicates a loss of the tissue's regenerative potential (Davis et al. 2021). IHC data confirmed the presence and effect of Stempeucel® at higher doses, as evidenced by the elevated expression of key regenerative markers, including Col-II and SOX9. The treatment downregulates the expression of cellular fibrosis (Col-I) in the NP cells. Following needle puncture, there is a notable increase in the expression of fibrotic marker Col-I and transformation of NP cells. This upregulation reflects a phenotypic shift from a healthy state to a more fibrotic and degenerative profile (Chen et al. 2023; Lin et al. 2020), contributing to the disruption of normal ECM composition and biomechanical integrity of the disc. However, treatment with the injectable Stempeucel® markedly downregulates Col-I expression in NP cells during the later stages of degeneration, suggesting its potential to mitigate fibrotic remodeling and support tissue regeneration. Stempeucel® enhances ECM composition in NP cells by promoting the synthesis of both large and small proteoglycans. In the needle puncture group, progressive destabilization of the ECM is evident, characterized by a significant reduction in the expression of key structural components (most notably ACAN), a major large proteoglycan critical for maintaining the hydration and mechanical properties of the NP (Empere et al. 2023), and its depletion severely compromises disc function (Sivan et al. 2014). Additionally, the expression of small leucine-rich proteoglycans (SLRP) TSUKUSHI or TSK is also downregulated following treatment, further contributing to ECM disorganization and impaired tissue integrity (Chen et al. 2017). Here, the injectable Stempeucel® enhances the ECM composition of NP cells by stimulating the synthesis of both large and small proteoglycans, such as ACAN, and TSK respectively.

Conclusion

In summary, we report that the lateral incision approach is an effective way for intradiscal delivery in the lumbar region. These findings suggest that Stempeucel® combined with HA represents a promising therapeutic approach for IVDD. The treatment not only alleviated pain but also promoted regeneration of the disc, as evidenced by the marked upregulation of chondrogenic markers and maintenance of disc structure. This aligns with previous studies highlighting the regenerative and chondro-protective properties of Stempeucel®. The comprehensive approach, incorporating behavioral assessments and detailed histological analysis, strengthens the validity of the model and the potential applicability of the treatment clinically.

Although the findings suggest the Stempeucel® alleviated pain, improved gait and histological features, and improved key chondrogenic and ECM markers. Still there is a room for improvement, such as the study lacking advanced imaging techniques, and detailed mechanistic investigations. Also, the study was performed in rodents which is lacks the translational relevance as the large animal models would be more appropriate.

Declarations

Acknowledgements

All the authors would like to acknowledge Director of NIPER-A for providing the necessary facilities for publishing this manuscript draft. The abstract of this study was presented at the International Society for Cell & Gene Therapy (ISCT) conference from 7-10 May 2025, in New Orleans, USA.

Author contribution

Gyanoday Tripathi: Data curation, Investigation, Methodology, Writing – original draft. **Komal Bhombe:** Methodology, Investigation. **Priyabrata Sarangi:** Investigation. **Suresh Kannan:** Conceptualization, data curation, Validation, **Pawan Kumar Gupta:** Conceptualization, Supervision, **Uday Kumar:** Investigation, Validation, **Hemant Kumar:** Conceptualization; Funding acquisition; Supervision; Writing – review & editing. The authors read and approved the final manuscript.

Funding

This study was financially supported by Stempeutics Research PVT. LTD. (Project ID: NIPER A/2023/CNS/02) and NIPER-Ahmedabad. The paid version of biorender.com was utilized to prepare the illustration.

Data availability

All data are provided with the manuscript and can be requested from the corresponding author upon reasonable request.

Conflict of interest

This study was supported by a research grant from Stempeutics Research PVT. LTD, which develops and commercialize the stem cell therapy evaluated in this research. The authors confirm that the study adhered to established scientific and ethical standards. Beyond the disclosed research funding, the authors declare no additional personal associations, competing financial/non-financial interests that could influence the design, interpretation, or reporting of the study findings.

Ethical approval

This study involving human samples which was approved by the Institutional Ethics Committee (IEC) of Kasturba Hospital, Manipal, Karnataka (Approval No. SRPL/CLI/07-08/001), and written informed consent was obtained from all donors. Animal experiments were conducted in accordance with ethical guidelines and were approved by the Institutional Animal Ethics Committee (NIPERA/IAEC/2023/018) at NIPER Ahmedabad, India.

References

1. Alfalogy E, Mahfouz S, Elmedany S, Hariri N, Fallatah S (2023) Chronic Low Back Pain: Prevalence, Impact on Quality of Life, and Predictors of Future Disability. Cureus 15(9):e45760. 10.7759/cureus.45760

2. Alkhatib B, Rosenzweig DH, Krock E, Roughley PJ, Beckman L, Steffen T, Weber MH, Ouellet JA, Haglund L (2014) Acute mechanical injury of the human intervertebral disc: link to degeneration and pain. European cells & materials 28:98–110; discussion 110–111. 10.22203/ecm.v028a08
3. Bergmann W, de Cv L, Plomp S, Vernooij JC, Wijnberg ID, Back W, Gröne A, Delany MW, Caliskan N, Tryfonidou MAJVP (2022) Intervertebral disc degeneration in warmblood horses: histological and biochemical characterization. 59(2):284–298
4. Binch AL, Fitzgerald JC, Growney EA, Barry FJNRR (2021) Cell-based strategies for IVD repair: clinical progress and translational obstacles. 17(3):158–175
5. Bonin RP, Bories C, De Koninck YJM (2014) A simplified up-down method (SUDO) for measuring mechanical nociception in rodents using von Frey filaments. 10:1744-8069-1710-1726
6. Česnik AB, Švajger U (2024) The issue of heterogeneity of MSC-based advanced therapy medicinal products-a review. Front cell Dev biology 12:1400347. 10.3389/fcell.2024.1400347
7. Chen L, Liao J, Klineberg E, Leung VY, Huang SJJTE, Medicine R (2017) Small leucine-rich proteoglycans (SLRPs): characteristics and function in the intervertebral disc. 11(3):602–608
8. Chen S, Chen M, Wu X, Lin S, Tao C, Cao H, Shao Z, Xiao G (2022) Global, regional and national burden of low back pain 1990–2019: A systematic analysis of the Global Burden of Disease study 2019. J Orthop translation 32:49–58. 10.1016/j.jot.2021.07.005
9. Chen X, Wang Z, Deng R, Yan H, Liu X, Kang RJIR (2023) Intervertebral disc degeneration and inflammatory microenvironment: expression, pathology, and therapeutic strategies. 72(9):1811–1828
10. Cheng Z, Li Y, Zeng W, Liang Y, Huang J, Huang J, Lu S, Li M, Huang L (2021) A Novel Extreme Lateral Approach. for Needle Puncture Model of Lumbar Disc Degeneration in SD Rats
11. Chou A, Reza A, Choug C, Nicoll SJB (2003) Differential collagen expression by outer and inner annulus fibrosus and nucleus pulposus cells seeded in 3-d polymer scaffolds. 33:685–693
12. Davis S, Roldo M, Blunn G, Tozzi G, Roncada TJFB (2021) Biotechnology Influence of the mechanical environment on the regeneration of osteochondral defects. 9:603408
13. Di Sarno L (2022) In vitro hBM-MSCs characterization and differentiation on the scaffold for bone regenerative medicine
14. Diwan AD, Melrose JJJS (2023) Intervertebral disc degeneration and how it leads to low back pain. 6 (1):e1231
15. El-Jawhari JJ, Ganguly P, Jones E, Giannoudis PV (2021) Bone Marrow Multipotent Mesenchymal Stromal Cells as Autologous Therapy for Osteonecrosis: Effects of Age and Underlying Causes. Bioeng (Basel Switzerland) 8(5). 10.3390/bioengineering8050069
16. Empere M, Wang X, Prein C, Aspberg A, Moser M, Oohashi T, Clausen-Schaumann H, Aszodi A, Alberton PJFB, Biotechnology (2023) Aggrecan governs intervertebral discs development by providing critical mechanical cues of the extracellular matrix. 11:1128587

17. Glaeser JD, Tawackoli W, Ju DG, Yang JH, Kanim LE, Salehi K, Yu V, Saidara E, Vit JP, Khnkoyan Z, NaPier Z, Stone LS, Bae HW, Sheyn D (2020) Optimization of a rat lumbar IVD degeneration model for low back pain. JOR Spine 3(2):e1092. 10.1002/jsp2.1092
18. Gómez-Barrena E, Padilla-Eguiluz NG, Avendaño-Solá C, Payares-Herrera C, Velasco-Iglesias A, Torres F, Rosset P, Gebhard F, Baldini N, Rubio-Suarez JCJSCI (2018) A multicentric, open-label, randomized, comparative clinical trial of two different doses of expanded hBM-MSCs plus biomaterial versus iliac crest autograft, for bone healing in nonunions after long bone fractures: Study Protocol. 2018 (1):6025918
19. Gorney A, Blau S, Dohse C, Griffith E, Williams K, Lim JH, Knazovicky D, Lascelles B, Olby NJJVIM (2016) Mechanical and thermal sensory testing in normal chondrodystrophoid dogs and dogs with spinal cord injury caused by thoracolumbar intervertebral disc herniations. 30(2):627–635
20. Gruber HE, Sage EH, Norton HJ, Funk S, Ingram J, Hanley C Jr (2005) Targeted deletion of the SPARC gene accelerates disc degeneration in the aging mouse. 53(9):1131–1138
21. Jiang W, Glaeser JD, Kaneda G, Sheyn J, Wechsler JT, Stephan S, Salehi K, Chan JL, Tawackoli W (2023) Intervertebral disc human nucleus pulposus cells associated with back pain trigger neurite outgrowth in vitro and pain behaviors in rats. 15(725):eadg7020Avalos PJStm
22. Kannan S, Gokul Krishna S, Gupta PK, Kolkundkar UK (2024) Advantages of pooling of human bone marrow-derived mesenchymal stromal cells from different donors versus single-donor MSCs. Sci Rep 14(1):12654. 10.1038/s41598-024-62544-8
23. Khalid S, Ekram S, Ramzan F, Salim A, Khan IJFM (2023) Co-regulation of Sox9 and TGF β 1 transcription factors in mesenchymal stem cells regenerated the intervertebral disc degeneration. 10:1127303
24. Koroth J, Buko EO, Abbott R, Johnson CP, Ogle BM, Stone LS, Ellingson AM (2023) Bradley EWJIjoms Macrophages and intervertebral disc degeneration. 24 (2):1367
25. Kusuma GD, Carthew J, Lim R, Frith JE (2017) Effect of the Microenvironment on Mesenchymal Stem Cell Paracrine Signaling: Opportunities to Engineer the Therapeutic Effect. 26(9):617–631. 10.1089/scd.2016.0349
26. Lai A, Gansau J, Gullbrand SE, Crowley J, Cunha C, Dudli S, Engiles JB, Fusellier M, Goncalves RM, Nakashima DJJ (2021) Development of a standardized histopathology scoring system for intervertebral disc degeneration in rat models: An initiative of the ORS spine section. 4(2):e1150
27. Lai A, Moon A, Purmessur D, Skovrlj B, Winkelstein BA, Cho SK, Hecht AC, Iatridis JC (2015) Assessment of functional and behavioral changes sensitive to painful disc degeneration. J Orthop research: official publication Orthop Res Soc 33(5):755–764. 10.1002/jor.22833
28. Lee M, Kim B-J, Lim EJ, Back SK, Lee J-H, Yu S-W, Hong S-H, Kim JH, Lee S-H, Jung W-WJA, Analgesia (2009) Complete Freund's adjuvant-induced intervertebral discitis as an animal model for discogenic low back pain. 109(4):1287–1296
29. Leung VY, Chan WC, Hung SC, Cheung KM, Chan D (2009) Matrix remodeling during intervertebral disc growth and degeneration detected by multichromatic FAST staining. J Histochem

cytochemistry: official J Histochem Soc 57(3):249–256. 10.1369/jhc.2008.952184

30. Lin C-Y, Crowley ST, Uchida S, Komaki Y, Kataoka K, Itaka K (2019a) Treatment of Intervertebral Disk Disease by the Administration of mRNA Encoding a Cartilage-Anabolic Transcription Factor. Mol Therapy - Nucleic Acids 16:162–171. https://doi.org/10.1016/j.omtn.2019.02.012
31. Lin CY, Crowley ST, Uchida S, Komaki Y, Kataoka K, Itaka K (2019b) Treatment of Intervertebral Disk Disease by the Administration of mRNA Encoding a Cartilage-Anabolic Transcription Factor. Mol therapy Nucleic acids 16:162–171. 10.1016/j.omtn.2019.02.012
32. Lin D, Alberton P, Delgado Caceres M, Prein C, Clausen-Schaumann H, Dong J, Aszodi A, Shukunami C, Iatridis JC, Docheva DJAC (2020) Loss of tenomodulin expression is a risk factor for age-related intervertebral disc degeneration. 19(3):e13091
33. Lü D-S, Shono Y, Oda I, Abumi K, Kaneda KJS (1997) Effects of Chondroitinase ABC and Chymopapain on Spinal Motion Segment Biomechanics: An: In Vivo: Biomechanical, Radiologic, and Histologic Canine Study. 22(16):1828–1834
34. O'Connor KCJSCI (2019) Molecular profiles of cell-to-cell variation in the regenerative potential of mesenchymal stromal cells. 2019 (1):5924878
35. Oehme D, Goldschlager T, Rosenfeld J, Danks A, Ghosh P, Gibbon A, Jenkin GJTSWJ (2012) Lateral surgical approach to lumbar intervertebral discs in an ovine model. 2012
36. Olby N, Griffith E, Levine J (2020) Comparison of Gait Assessment Scales in Dogs with Spinal Cord Injury from Intervertebral Disc Herniation. J Neurotrauma 37(18):1991–1998. 10.1089/neu.2019.6804
37. Ouzin M, Kogler G (2023) Mesenchymal Stromal Cells: Heterogeneity and Therapeutical Applications. Cells 12(16). 10.3390/cells12162039
38. Penolazzi L, Lambertini E, D'Agostino S, Pozzobon M, Notarangelo MP, Greco P, De Bonis P, Nastruzzi C, Piva RJLS (2022) Decellularized extracellular matrix-based scaffold and hypoxic priming: A promising combination to improve the phenotype of degenerate intervertebral disc cells. 301:120623
39. Samanta A, Lufkin T, Kraus P (2023) Intervertebral disc degeneration-Current therapeutic options and challenges. Front public health 11:1156749. 10.3389/fpubh.2023.1156749
40. Shapiro IM, Risbud MV (2016) Intervertebral Disc. Springer
41. Sivan SS, Wachtel E, Roughley PJBBA-GS (2014) Structure, function, aging and turnover of aggrecan in the intervertebral disc. 1840(10):3181–3189
42. Steffen F, Smolders LA, Roentgen AM, Bertolo A, Stoyanov JJTEPCM (2017) Bone marrow-derived mesenchymal stem cells as autologous therapy in dogs with naturally occurring intervertebral disc disease: feasibility, safety, and preliminary results. 23(11):643–651
43. Widjaja G, Jalil AT, Budi HS, Abdelbasset WK, Efendi S, Suksatan W, Rita RS, Satria AP, Aravindhan S, Saleh MM, Shalaby MN, Yumashev AV (2022) Mesenchymal stromal/stem cells and their exosomes application in the treatment of intervertebral disc disease: A promising frontier. Int Immunopharmacol 105:108537. 10.1016/j.intimp.2022.108537

44. Willer H, Spohn G, Morgenroth K, Thielemann C, Elvers-Hornung S, Bugert P, Delorme B, Giesen M, Schmitz-Rixen T, Seifried E, Pfarrer C, Schäfer R, Bieback K (2022) Pooled human bone marrow-derived mesenchymal stromal cells with defined trophic factors cargo promote dermal wound healing in diabetic rats by improved vascularization and dynamic recruitment of M2-like macrophages. Front Immunol 13:976511. 10.3389/fimmu.2022.976511
45. Yang S, Zhang F, Ma J, Ding W (2020) Intervertebral disc ageing and degeneration: The antiapoptotic effect of oestrogen. Ageing Res Rev 57:100978. 10.1016/j.arr.2019.100978
46. Zhang Y, Zhang Z, Chen P, Ma CY, Li C, Au TYK, Tam V, Peng Y, Wu R, Cheung KMC, Sham PC, Tse H-f, Chan D, Leung VY, Cheah KSE, Lian Q (2020) Directed Differentiation of Notochord-like and Nucleus Pulposus-like Cells Using Human Pluripotent Stem Cells. Cell Rep 30(8):2791–2806e2795. https://doi.org/10.1016/j.celrep.2020.01.100

Figures

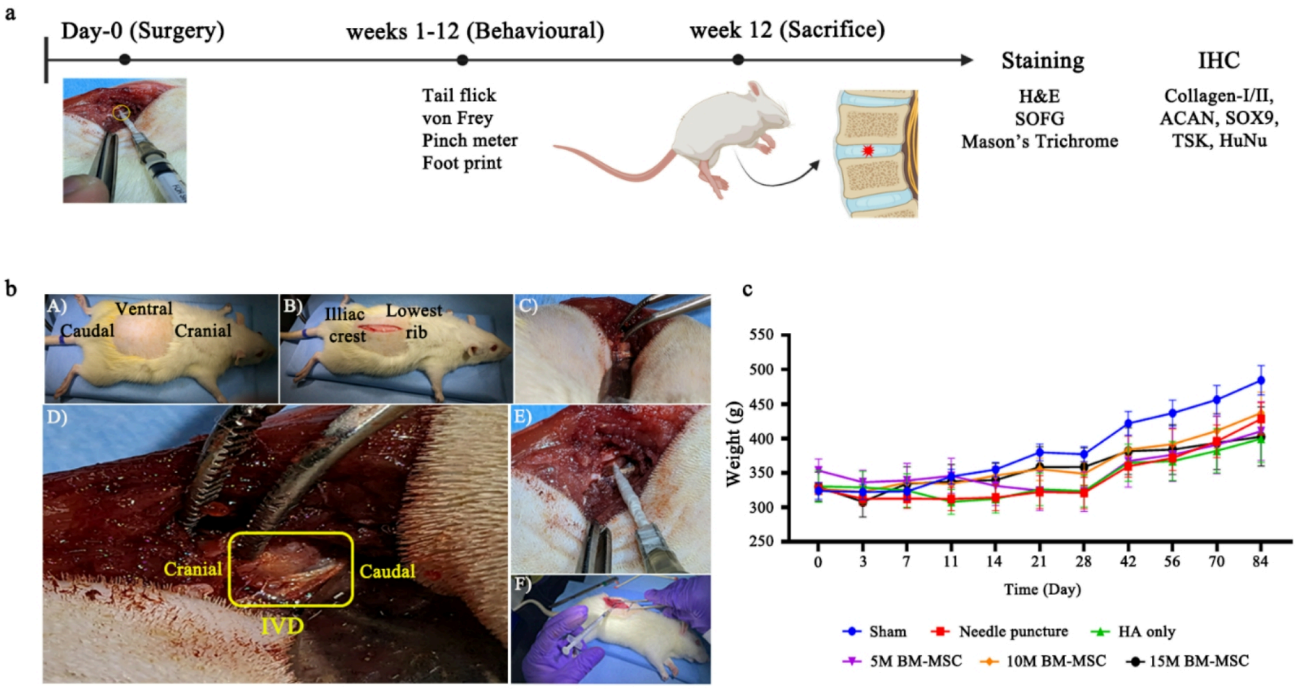

Figure 1

No significant alterations in body weight following needle puncture and subsequent treatment with Stempeucel®.(a) Represents the experimental design. (b) Surgical procedure of lateral incision approach of needle puncture. (c) Body weight assessment days 0 to 84 (n=6). Data represent body weight assessments at days 0, 3, 7, 11, 14, 21, 28, 42, 56, 70, and 84 after lumbar disc puncture. Two-way

ANOVA, followed by Tukey's Multiple Comparison Test as post hoc evaluation, was performed for statistical analysis. Results are presented as mean ± SEM.

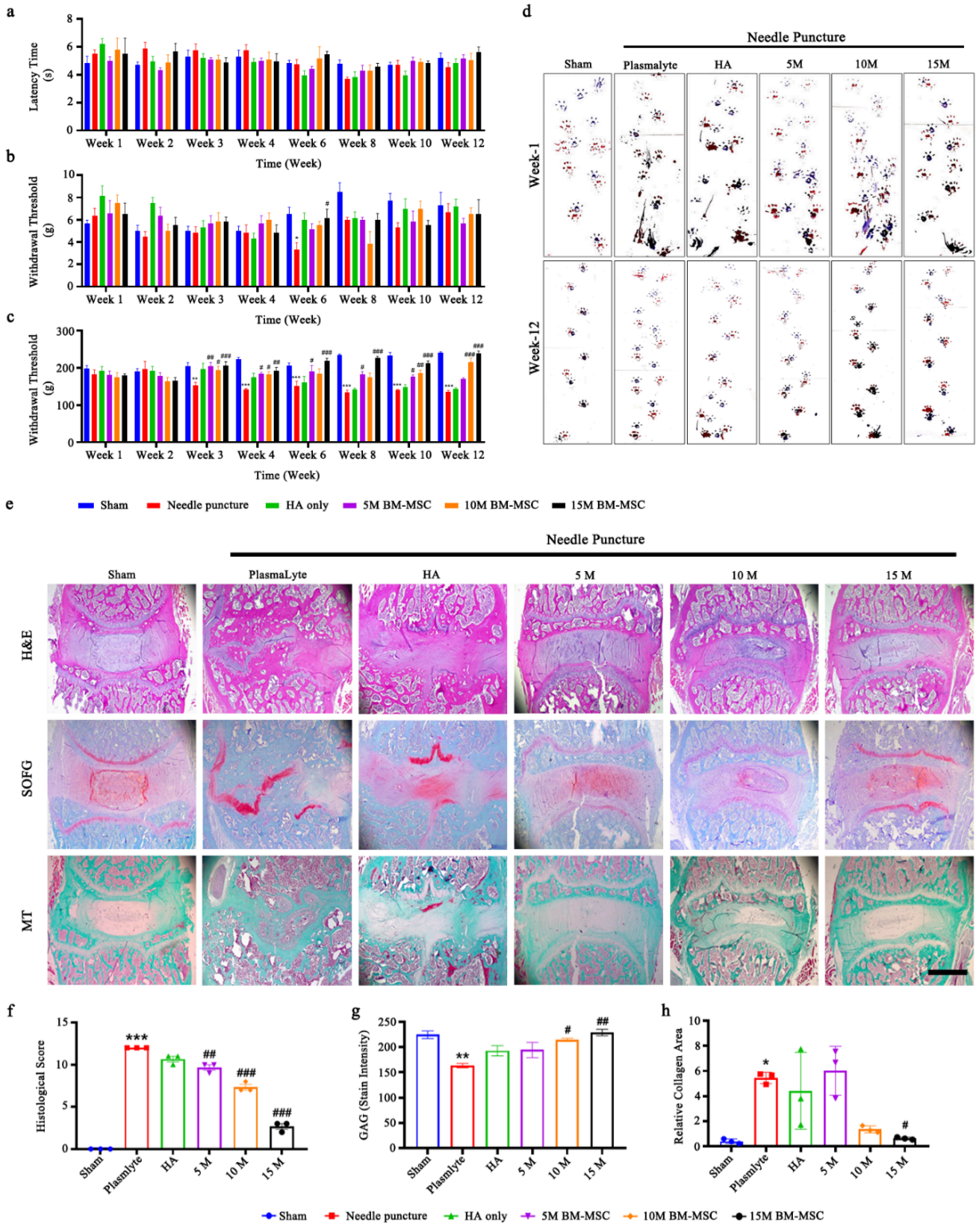

Figure 2

Higher doses of Stempeucel® significantly reduce pain perception, enhance gait behavior, and improve histological features in the later stages of injury. (a) Graph represents tail withdrawal latency time, (b)

mechanical allodynia, (c) paw withdrawal threshold of hind paw (n=6). Data are represented as mean ± SEM. Data represent pain behaviour assessments at weeks 1, 2, 3, 4, 6, 8, 10, and 12 after lumbar disc puncture, comparing sham with injury and treatment groups (n=6). Statistical analysis was conducted using two-way ANOVA, followed by Tukey's Multiple Comparison Test for post hoc analysis. Data are presented as mean ± SEM. ***p < 0.01*: Sham vs Injury (Week 3), ***p < 0.01*: Sham vs Injury (Week 6), ****p < 0.001*: Sham vs Injury (Weeks 4, 8, 10, and 12), *#p < 0.05*: Injury vs Treatment 10M (Week 3); Treatment 5M and 10M (Week 4), *##p < 0.01*: Injury vs Treatment 5M (Week 3); Treatment 15M (Week 6), *###p < 0.001*: Injury vs Treatment 15M (Weeks 4, 8, 10, and 12). (d) Assessment of gait behaviour by footprint method at weeks 1 and 12, comparing sham with injury and treatment groups. (e) Assessment of tissue morphology, proteoglycan content, and collagen fibers was performed using H&E, SOFG, and MT staining in sham, PlasmaLyte, HA, and Stempeucel® treatment groups (5M, 10M, and 15M) at week 12 (scale bar: 400 µm). (f) Histological score of H&E staining (n=3). Statistical significance: ****p < 0.001* for Sham vs Injury, *##p < 0.01*for Injury vs 5M Treatment, and *###p < 0.001* for Injury vs 10M and 15M Treatments. (g) Quantification of GAG content (SOFG staining) n=3. Statistical significance: ***p < 0.01* for Sham vs Injury, *#p < 0.05*for Injury vs 10M Treatment, and *##p < 0.01* for Injury vs 15M Treatments. (h) Quantification of % collagen area (MT staining) n=3. Statistical significance: **p < 0.05* for Sham vs Injury, *#p < 0.05* for Injury vs 15M Treatment.

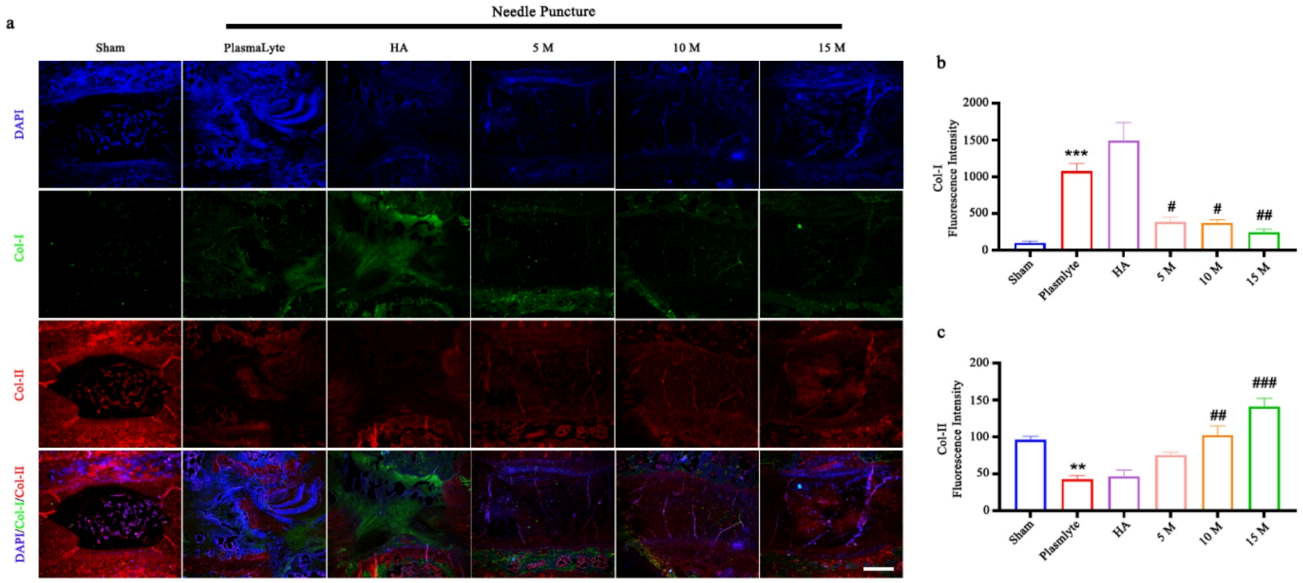

Figure 3

Effect of high-dose Stempeucel® on NP phenotype cells and cellular hypertrophy.(a) Representative IHC images of Col-I and II, at week 12, used to assess fibrosis and the presence of phenotype cells in the NP region across all experimental groups. (b) % mean fluorescence intensity of Col-I (scale bar: 100 µm). Statistical significance: ****p < 0.001* for Sham vs Injury, *#p < 0.05*for Injury vs Treatment 5M and 10M,

##p < 0.01 for Injury vs Treatment 15M. (c) % mean fluorescence intensity of Col-II (n=3). Statistical analysis was performed using one-way ANOVA followed by Tukey's Multiple Comparison Test. Data are presented as mean ± SEM. Significance: ***p < 0.01* represents Sham vs Injury, *##p < 0.01* represents Injury vs Treatment 10M, *###p < 0.001*represents Injury vs Treatment 15M.

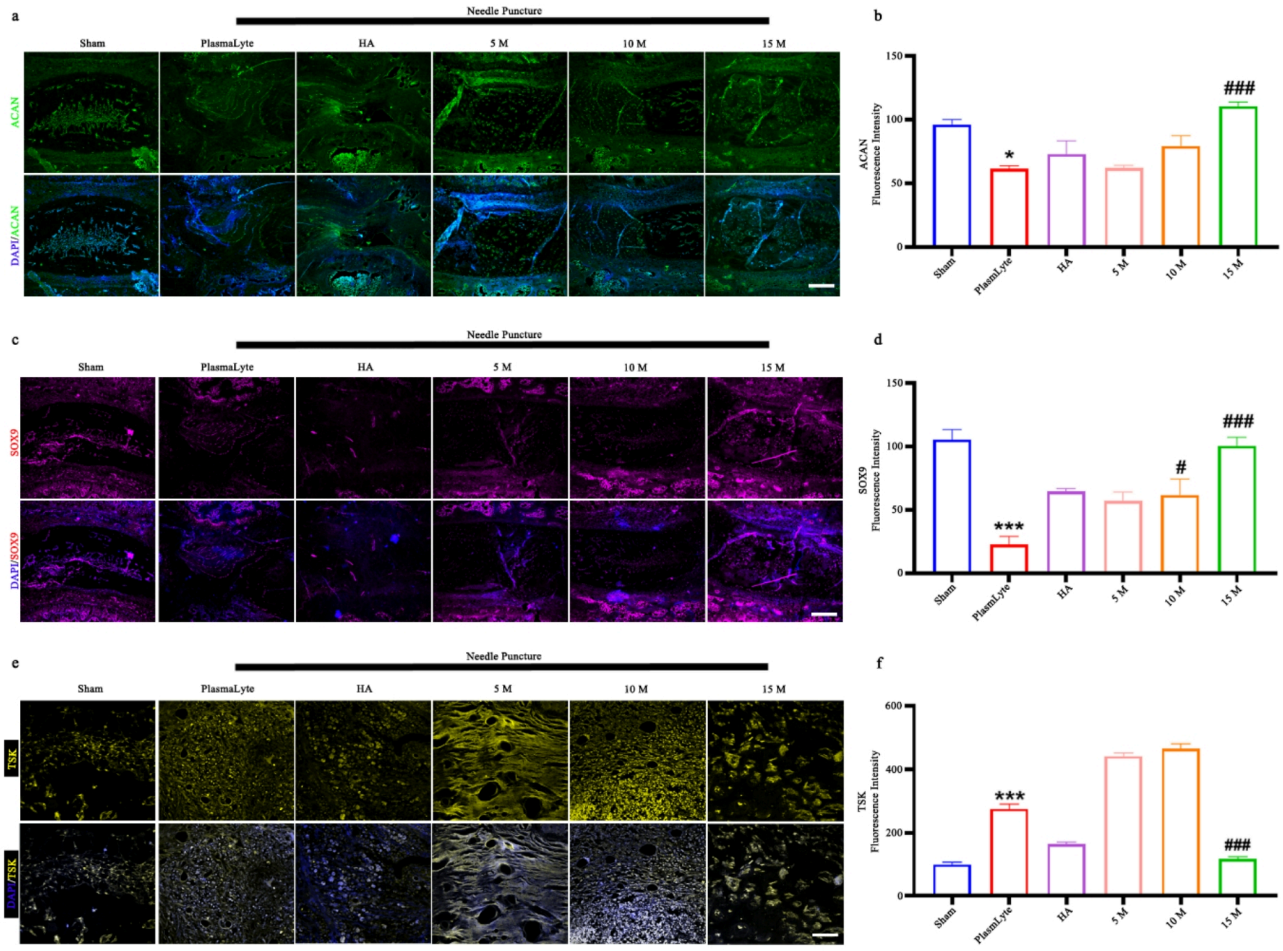

Figure 4

Effect of high-dose Stempeucel® on large and small proteoglycans, and chondrogenesis. (a) Representative IHC images of ACAN, (b) % mean fluorescence intensity of ACAN (n=3). scale bar: 100 µm. ****p < 0.001* represents Sham vs Injury, *###p < 0.001*represents Injury vs Treatment 15M. (c) SOX9 in the NP region of sham, injury, HA, 5M, 10M, and 15M at week 12. (d) % mean fluorescence intensity of SOX9 (n=3) scale bar: 100 µm. (e) TSK for the assessment of TSK in the ECM of NP region. (f) % mean fluorescence intensity of TSK (n=3, scale bar: 25 µm). ****p < 0.001* represents Sham vs Injury, *#p < 0.05*represents Injury vs Treatment 10M, *###p < 0.001* represents Injury vs Treatment 15M. Statistical analysis was carried out by one-way ANOVA, followed by post hoc analysis by Tukey's Multiple Comparison Test. Data are represented as mean ± SEM.

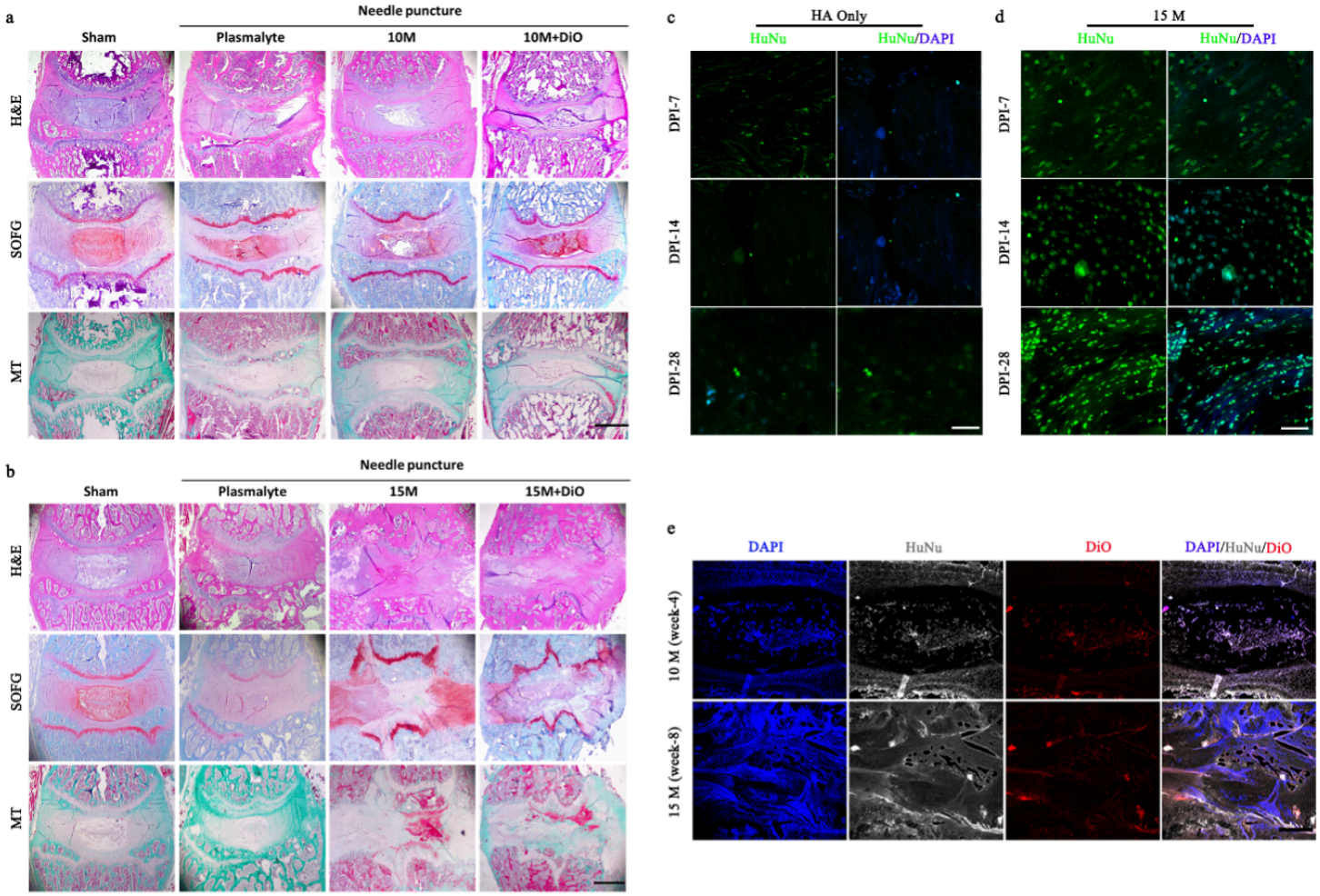

Figure 5

(a) Assessment of morphology, proteoglycan content, and collagen fibers through H&E, SOFG, and MT staining at weeks 4 of the sham, PlasmaLyte, 10M, 10M+DiO followed by (b) at weeks 8 sham, PlasmaLyte, 15M, 15M+DiO (scale bar: 400 μm). (c-d) IHC images stained with DAPI, and HuNu, at days 7, 14, and 28 for the assessment of the presence of hBM-MSCs in IVDs of HA and hBM-MSCs treated groups (scale bar: 50 μm). (e) Results of IHC images stained with DAPI, HuNu, and DiO at weeks 4 (10 million) and 8 (15 million) for the assessment of the presence of hBM-MSCs in all the experimental groups. Scale bar: 200 μm (n=8/week).

Supplementary Files

This is a list of supplementary files associated with this preprint. Click to download.

- floatimage1.jpeg
- SupplementaryInformation.docx